



Far-field triggering of foreshocks near the nucleation zone of the 5 September 2012 (M_W 7.6) Nicoya Peninsula, Costa Rica earthquake



Jacob I. Walter^{a,*}, Xiaofeng Meng^b, Zhigang Peng^b, Susan Y. Schwartz^c,
Andrew V. Newman^b, Marino Protti^d

^a Institute for Geophysics, University of Texas at Austin, Austin, TX, United States

^b School of Earth and Atmospheric Sciences, Georgia Institute of Technology, Atlanta, GA, United States

^c University of California, Santa Cruz, Department of Earth and Planetary Sciences, Santa Cruz, CA, United States

^d Observatorio Vulcanológico y Sismológico de Costa Rica, Universidad Nacional, Heredia, Costa Rica

ARTICLE INFO

Article history:

Received 15 June 2015

Received in revised form 11 September 2015

Accepted 12 September 2015

Available online 26 September 2015

Editor: P. Shearer

Keywords:

foreshocks
seismicity
slow slip
megathrust earthquake

ABSTRACT

On 5 September 2012, a moment magnitude (M_W) 7.6 earthquake occurred directly beneath the Nicoya Peninsula, an area with dense seismic and geodetic network coverage. The mainshock ruptured a portion of a previously identified locked patch that was recognized due to a decade-long effort to delineate the megathrust seismic and aseismic processes in this area. Here we conduct a comprehensive study of the seismicity prior to this event utilizing a matched-filter analysis that allows us to decrease the magnitude of catalog completeness by 1 unit. We observe a statistically significant increase in seismicity rate below the Nicoya Peninsula following the 27 August 2012 (M_W 7.3) El Salvador earthquake (about 450 km to the northwest and 9 days prior to the Nicoya earthquake). Additionally, we identify a cluster of small-magnitude (<2.2) earthquakes preceding the mainshock by about 35 min and within 15 km of its hypocenter. The immediate foreshock sequence occurred in the same area as those earthquakes triggered shortly after the El Salvador event; though it is not clear whether the effect of triggering from the El Salvador event persisted until the foreshock sequence given the uncertainties in seismicity rates from a relatively small number of earthquakes. If megathrust earthquakes at such distances can induce significant increases in seismicity during the days before another larger event, this sequence strengthens the need for real-time seismicity monitoring for large earthquake forecasting.

© 2015 Elsevier B.V. All rights reserved.

1. Introduction

The hallmark mechanical process that defines an earthquake is the unstable and rapid rupture that propagates across a frictional fault interface. Both laboratory (Dieterich, 1979) and numerical experiments (Ampuero and Rubin, 2008) find that slow and accelerating fault slip often precedes the fast rupture. However, identifying such nucleation processes preceding large earthquakes is extremely difficult, likely due to a lack of geodetic instrumentation in close proximity to the source (Roeloffs, 2006). This is particularly problematic in subduction zones, where the seismogenic fault generally occurs offshore (Newman, 2011). One possible indicator of such a preparation process is foreshocks (Mogi, 1963; Jones and Molnar, 1979), which consist of seismic activity that occurs very close to and immediately before a larger event. In some instances, such seismicity and slow slip appear to be sustained

for weeks prior to a large earthquakes, including the recent 2011 Tohoku–Oki (e.g. Kato et al., 2012) and 2014 Iquique earthquakes (Brody and Lay, 2014; Kato and Nakagawa, 2014), raising questions about the appropriate spatial and temporal scales over which to consider such preparatory processes for large megathrust earthquakes.

The exact relationship between foreshocks and mainshock nucleation is still in debate (Mignan, 2014). Some studies considered foreshocks as a reflection of an aseismic process that ultimately initiated the mainshock rupture (Dodge et al., 1995; McGuire et al., 2005). Small foreshocks in these cases may represent small asperities breaking during the initial stage of a slow slip event (*the pre-slip model*). The slow slip itself may occur below the detection threshold of modern geodetic networks, especially if it occurs offshore or near/below the brittle–ductile transition. Another conceptual model does not require initial slow slip, but relies on the assumption that any earthquake can trigger subsequent events. There is a small probability that “aftershocks” of higher magnitude than the triggering mainshock could occur (Helmstetter et al., 2003; Felzer et al., 2004). In this case, the triggering mainshock becomes

* Corresponding author.

E-mail address: jwalter@ig.utexas.edu (J.I. Walter).

the ‘foreshock’. Thus, seismic activity can build and subsequently trigger rupture of a large earthquake in a so-called *earthquake cascade model*.

Recent observations of foreshock sequences before several large earthquakes indicate that their ruptures were preceded by increasing or migrating foreshocks along the plate interface, favoring the pre-slip model. Foreshock activity in the hour prior to the 1999 M_W 7.4 Izmit mainshock led Bouchon et al. (2011) to infer that this earthquake was preceded by slow-slip that prompted the unstable mainshock rupture. Kato et al. (2012) reported two sequences of migrating foreshocks of the great 2011 Tohoku–Oki (M_W 9) earthquake and interpreted them as driven by slow-slip transients propagating toward and leading up to rupture initiation. Stress loading from the second sequence, which involved large slip rates, was identified as the probable trigger of unstable dynamic rupture of the mainshock. Precursory slow slip that involved 2–3 cm of vertical deformation over 5–7 days was confirmed a few weeks prior to the 2011 Tohoku–Oki mainshock by measurements of absolute pressure gauges (APG) deployed on the seafloor (Ito et al., 2013). The 2014 Iquique, Chile megathrust earthquake was preceded by shallow plate boundary events that migrated toward the mainshock initiation in the two weeks leading up to it (Kato and Nakagawa, 2014). The 1990 Nicoya Gulf earthquake, which occurred south of the Nicoya Peninsula and under plausibly similar interface conditions as the 2012 event, was preceded by small foreshocks 15 h before the mainshock (Protti et al., 1995).

However, other recent studies have failed to find clear evidence of foreshock migration and/or increase right before large earthquakes (Doi and Kawakata, 2012; Wu et al., 2014) and earthquake swarm activity does not always culminate in a mainshock (Holtkamp et al., 2011). Brodsky and Lay (2014) suggested that the tectonic context of swarm activity might aid in evaluating its potential to culminate in a mainshock. They noted that migrating earthquake sequences occurring in seismic gaps within geodetically locked regions ended up as foreshocks to mainshock rupture, whereas other swarm activity did not.

Bouchon et al. (2013) found that ~70% of interplate earthquakes are preceded by extended sequences of seismic activity up to months prior to the subsequent event, indicating a relatively long precursory phase. But a recent study suggested that the apparent behavior could be explained solely by the cascade model (Felzer et al., 2015). One potential issue is that the magnitude of completeness, M_C (e.g. Section 3.1) for most foreshock sequences is relatively high (~3.0). Hence, the underlying spatio-temporal evolutions are not well identified when the local microseismicity is not adequately known. An effective way to identify more small events and reduce M_C is the matched-filter technique (Shelly et al., 2007). This technique utilizes waveforms or travel time information of known events as templates, or “matched filters,” to search for similar patterns in the continuous recordings. It has been successfully applied to detect many unreported events that occurred at mid-ocean ridges and transform faults (Shearer, 1994), track low-frequency earthquakes within the deep tectonic tremor signals (Shelly et al., 2007; Brown et al., 2008; Shelly and Hardebeck, 2010) and earthquake swarms (Shelly and Hill, 2011), detect early aftershocks (Peng and Zhao, 2009; Lengliné and Marsan, 2009; Lengliné et al., 2012), triggered earthquakes (Meng and Peng, in press; Yao et al., 2015), and foreshocks (Bouchon et al., 2011; Kato et al., 2012; Wu et al., 2014; Kato and Nakagawa, 2014).

In this study, we examine in detail the spatio-temporal evolution of seismicity preceding an M_W 7.6 megathrust earthquake on 5 September 2012 beneath the Nicoya Peninsula, Costa Rica. We choose this region because it was well instrumented/studied and some clear foreshocks have been identified in a recent study (Protti et al., 2014). Here we apply the matched filter method to detect possible missing events prior to the 2012 Nicoya mainshock,

and then examine their spatio-temporal evolution and relationship with other events/processes. We specifically examine whether an M_W 7.3 earthquake offshore southern El Salvador that occurred approximately 450 km northwest of the Nicoya earthquake and 9 days earlier (27 August 2012), increased the seismicity rate around the Nicoya Peninsula and promoted the earthquake’s occurrence.

2. Tectonic setting

Beneath the Nicoya Peninsula the Cocos and Caribbean plates converge at approximately 8.5 cm/yr (DeMets et al., 2010). This region has experienced numerous large earthquakes, including similar events to the 2012 earthquake in 1853, 1900, and 1950 (M 7.7) (Protti et al., 2001). Prior seismic, geodetic, and geomorphic studies had mapped the Nicoya segment as a locked zone, and the 2012 event was to some degree expected (Nishenko, 1991; Protti et al., 1995; Marshall and Anderson, 1995; Ghosh et al., 2008; Feng et al., 2012). Over the last 10 years, an international and multi-University network of GPS and seismic stations has operated on the Nicoya Peninsula (Dixon et al., 2014). Data from this network has been used to define heterogeneous interface structure (Kyriakopoulos et al., 2015), generate a model of plate coupling (Feng et al., 2012), to determine the coseismic slip distribution in the 2012 Nicoya earthquake (Yue et al., 2013; Protti et al., 2014) and to detect at least 7 slow slip events accompanied by tremor activity (Outerbridge et al., 2010; Walter et al., 2011, 2013; Jiang et al., 2012). Slow slip occurs repeatedly in regions both up and down-dip of the well-locked patch that ruptured in the 5 September 2012 earthquake (Dixon et al., 2014). This behavior suggests that relatively weak fault patches that produce slow-slip events can interact with relatively stronger adjacent zones capable of producing significant earthquakes. The degree to which slow slip relieves inter-seismic strain spatially and temporally is still not well understood in neither this region nor other subduction zones throughout the world. To resolve this, we focus on building a comprehensive catalog of the microseismicity immediately before a megathrust earthquake to better understand how the foreshock sequence starts.

3. Methods

3.1. Earthquake catalog and matched-filter technique

For the period beginning 30 days before through 50 days after the Nicoya mainshock we perform automatic earthquake detections using the Antelope seismic database tools (www.brrt.com). The method first uses an automatic short-term/long-term amplitude ratio filter to identify potential seismic phases that are then temporally correlated across network stations, and finally located within an initial one-dimensional earth model (IASPEI91). Subsequently, the phase arrivals are analyst-reviewed and additional phases are determined. The phase information is then used to relocate the events with TomoDD (Zhang and Thurber, 2003) utilizing a locally-developed three-dimensional velocity model (Moore-Driskell et al., 2013), as are done for other regional earthquakes recorded by local networks (Kyriakopoulos et al., 2015).

In order to run the matched-filter technique (Meng et al., 2013), we use the picked waveforms as initial templates. We bandpass filter these data between 5 to 15 Hz and cut the waveforms 1 s before and 5 s after the phase arrival (P or S). We utilize template events that consist of phase arrivals for at least 5 stations within the network. The technique computes the cross-correlation (CC) values between the template and continuous data at each sample point through time to obtain a CC function. The CC functions for all 3 components (when P and S phase picks are both apparent on a single station; only horizontal components when only S and only

vertical when only P) are then time-shifted back to the origin time and stacked for each component. Detection occurs when the stack exceeds 9 times the median absolute deviation (MAD), a threshold similar to other studies utilizing a network-based matched-filter (Shelly et al., 2007). We perform detection on the Oakridge National Laboratory's Keeneland GPU cluster using a code optimized for that system (Meng et al., 2012). An example of a waveform match between template and newly detected event is shown in supplemental material (Fig. S1). Following Peng and Zhao (2009), we estimate the magnitude of the newly detected events based on its median amplitude ratio with the template events.

Next we determine the magnitude of completeness M_C , which is the magnitude below which the log-linear Gutenberg–Richter empirical relationship becomes depleted in events. Thus, a seismicity catalog can be considered “complete” for earthquakes with magnitudes greater than M_C . We calculate M_C by the maximum curvature method as implemented in the ZMAP software package (Wiemer, 2001) and utilize these values to determine the degree to which our method improves the seismicity catalog.

3.2. Seismicity rate changes

To determine whether the seismicity rate changes due to external factors, we examine two methods. One is to calculate the β value showing the significance of seismicity rate change after a certain point in time (Matthews and Reasenber, 1988; Marsan and Wyss, 2011), which is defined by:

$$\beta = \frac{N_a - N_b \frac{\Delta t_a}{\Delta t_b}}{\sqrt{N_b \frac{\Delta t_a}{\Delta t_b}}}$$

where N_b is the number of earthquakes before the event during the time interval Δt_b and N_a is the number of earthquakes after the event during the time interval Δt_a . The β is essentially the observed number of earthquakes after a triggering event minus the expected number, normalized by the standard deviation. Typically β values greater than 2 indicate statistically significant increases in the seismicity rate (Hill and Prejean, 2007).

We also calculate the Z-statistic, also aimed to establish if seismicity rate changes occur and are positive ($Z > 2$) over an interval of time (Habermann, 1981). We use a modified version (Marsan and Wyss, 2011) such that:

$$Z = \frac{N_a \Delta t_b - N_b \Delta t_a}{\sqrt{N_a \Delta t_b^2 - N_b \Delta t_a^2}}$$

For the null hypothesis of no change in the seismicity rate, Z is distributed like a Gaussian with zero mean and standard deviation of 1. Since the null hypothesis falls within the normal standard deviation, then a value for $Z \geq 2$ is a statistically significant change (95% significance level) in the seismicity rate. The Z statistic is preferred in some studies of seismicity because time periods both before and after the particular interval of time are given equal weight in the denominator.

3.3. Tremor catalog

We identify and locate tremor between January 2012 and the September Nicoya mainshock using a modified version of the automated envelope cross-correlation algorithm of Wech and Creager (2008). We band-pass filter the east component in two frequency ranges between 1 to 5 Hz and 8 to 20 Hz, create envelope functions, low-pass filter at 0.1 Hz, and decimate to 1 Hz. We use a 2-minute time window, shifting with 50% overlap, to cross-correlate envelope functions and located tremor when CC values exceeded a value of .65 on more than 5 station pairs. To

eliminate local earthquakes from the tremor catalog, we did not locate tremor if CC values computed using the higher frequency envelopes also exceeded .65 on the same station pairs or was synchronous with a detected earthquake. We locate tremor using a 1-D local velocity model for the Nicoya area (DeShon et al., 2006) following Wech and Creager (2008), only allowing locations with epicentral bootstrapping error estimates less than 0.1 degrees; the tremor location method provides little constraint in depth and due to limited station coverage, we suspect that actual epicentral tremor location errors are greater than the bootstrap estimates. In order to further eliminate isolated earthquakes or randomly scattered erroneous detections, we apply a clustering requirement that each event has at least two additional events in 24 hours within 0.1 degrees.

4. Results

The matched-filter technique greatly improves our ability to detect smaller earthquakes. Fig. 1 shows 1566 pre-mainshock events determined through the matched-filter technique and color-coded according to time. In addition, the total number of early analyst-picked aftershocks does not vary significantly (with the exception of some additional analyst picks) from those reported in Protti et al. (2014). The early aftershocks shown in Fig. 1b were analyzed using methods described in that paper. After running the automatic detection algorithm and handpicking certain events, but before applying the matched-filter technique, we determine $M_C = 1.6$ for the period between day 220 (~30 days before the mainshock) and prior to the Nicoya mainshock (Fig. 2). The matched-filter method over this time period improves the value of M_C to 0.6, consistent with the order-of-magnitude M_C improvements gained in other datasets (Schaff and Waldhauser, 2010; Meng and Peng, in press). The estimated b-value also varies significantly between the catalogs, highlighting the importance of using complete catalog datasets for b-value studies, similar to what was done for Nicoya earthquakes in 2000 (Ghosh et al., 2008). Sometimes magnitude uncertainties are prevalent in local seismicity studies, including but not limited to poorly calibrated instruments and background noise contamination during robust aftershocks sequences. In addition, magnitude is averaged over the stations observing that particular event, often with error of ± 0.2 magnitude units. Due to these uncertainties that may also propagate into our matched-filter detections, we conservatively use a cutoff magnitude of 1.0 excluding lower values for the remainder of the seismicity rate change analysis. The M_C value should not change greatly through time, over the period evaluated here, as the seismic network configuration did not change between day 220 and the Nicoya mainshock. The 1566 pre-mainshock events shown in Fig. 1 are events where $M_L \geq M_C$.

We next examine spatio-temporal evolution of the newly augmented catalog, with special focus on the period of time prior to the Nicoya mainshock.

4.1. Distant triggering by the El Salvador earthquake

The M_W 7.3 El Salvador earthquake occurred 9 days before and approximately 450 km to the northwest of the mainshock nucleation of the Nicoya earthquake (Fig. 1a). Though smaller, Borrero et al. (2014) showed that it created a locally large tsunami (peak run-up of 6 m), exhibited little high-frequency shaking, and had an excessively long rupture duration (approximately 60 s), all indicative of a small ‘tsunami earthquake’ (Kanamori, 1972). A similar M_W 7.7 event that occurred immediately to the south across much of the Nicaraguan portion of the Middle America Trench in 1992 (e.g. Satake, 1994).

Following the El Salvador earthquake, we detect many earthquakes of magnitudes 1–2 occurred near the Nicoya Peninsula,

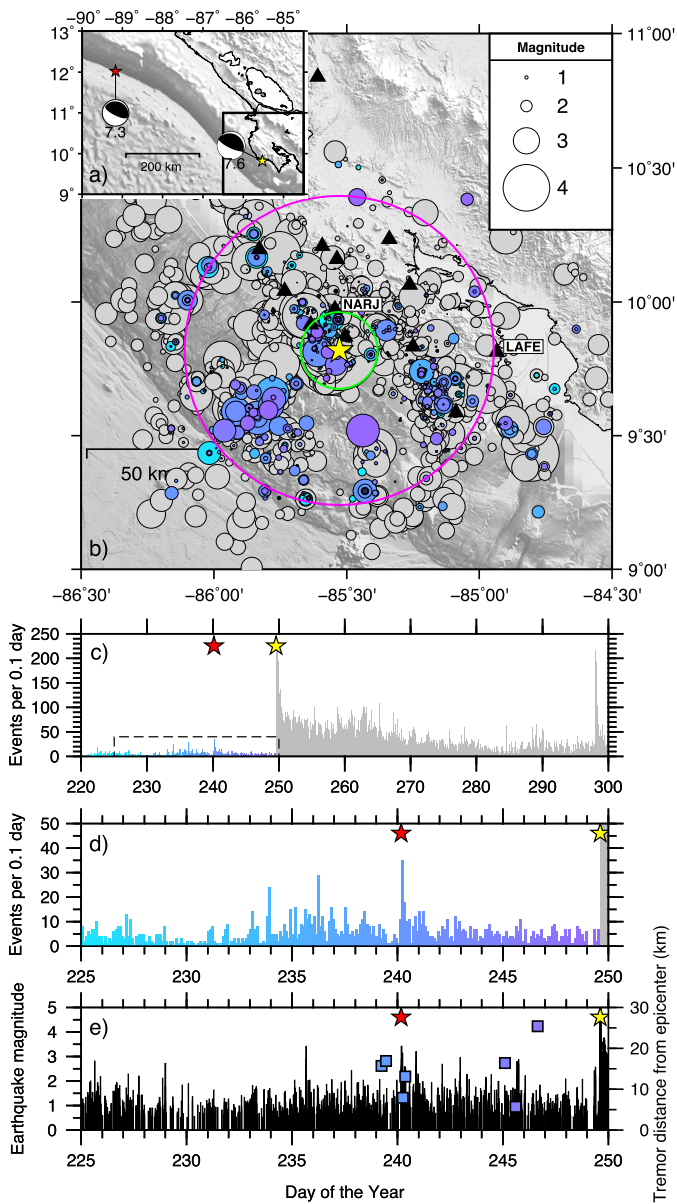


Fig. 1. Seismicity map for the time period around the 5 September 2012 Nicoya Peninsula earthquake, including aftershocks (Protti et al., 2014). (a) Inset map showing focal mechanisms and epicenters for the El Salvador (epicenter is red star) and Nicoya (epicenter is yellow star) earthquakes. (b) Map of the foreshock and early aftershock activity, where the black triangles indicate seismic stations. Size of the circle for earthquakes is relative to local magnitude and does not correspond to the map scale for comparing rupture area. The green and magenta circles are radii 15 and 60 km (see Fig. 3) from the mainshock nucleation point (9.8193, -85.5271), based on the network-observed initial P-wave arrivals. (c) Waveform-matching enhanced catalog of seismicity rate prior to the earthquake and the early aftershocks during the first 50 days after the mainshock. Dashed boxed area designates inset for 1d. (d) Zoom of time window from 1c, including seismic activity prior to the mainshock. Note the increase around the timing of the El Salvador earthquake (240.2 days). (e) Magnitude of events in the same time window, indicating no clear large-magnitude events prior to the mainshock. Squares correspond to detected tremor plotted as a function of time and distance from mainshock nucleation. (For interpretation of the references to color in this figure legend, the reader is referred to the web version of this article.)

in the 30 min after this distant earthquake and believe these to be dynamically triggered by the seismic waves of the El Salvador mainshock. These are present as an increase in seismicity in the matched-filter catalog (Fig. 1d) and are present upon inspection of the spectrogram from local station LAFE (Fig. 3; also for station NARJ in Fig. S2). The spectrogram reveals local Nicoya

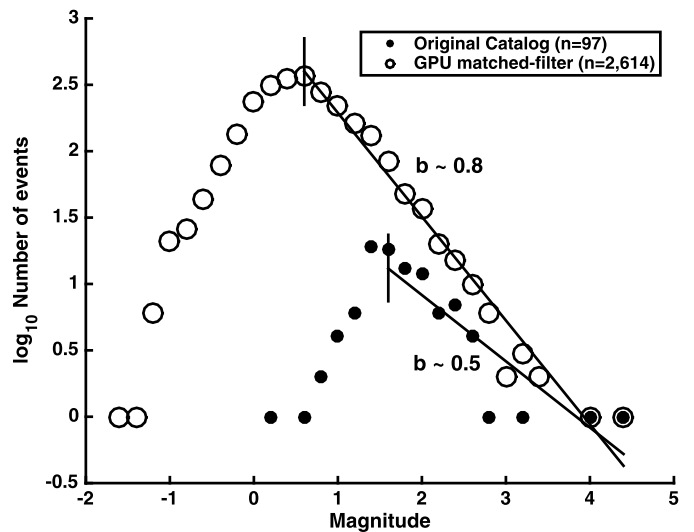


Fig. 2. Gutenberg–Richter distribution for the matched-filter catalog compared to the original catalog. The completeness magnitude, M_C , is indicated by vertical lines and is approximately 1.6 and 0.6 for the original and matched-filter catalogs, respectively. We choose a more conservative estimate of M_C of 1.0 for seismicity results obtained through the matched-filter catalog.

Peninsula seismicity during the surface and coda-waves of the El Salvador earthquake, and sporadically during the 2 hours following the event.

After Hill and Prejean (2007) we approximate the dynamic stress change, σ_d , using:

$$\sigma_d = G\dot{u}/v$$

where the peak ground velocity at various stations ($\dot{u} = 0.05\text{--}0.15$ cm/s) is measured, and nominal values for the shear modulus ($G = 30$ GPa) and phase velocity ($v = 3.5$ km/s) are used. We find σ_d to be approximately 10 kPa for shaking along the Nicoya Peninsula following the El Salvador earthquake. In order to more rigorously evaluate the seismicity rate change under this dynamic stress, we compute the rate change before and after the El Salvador event. We also estimate the seismicity rate at a range of distances from the mainshock epicenter.

Fig. 4 illustrates the possible changes in Z and β values calculated for seismicity with increasing radii (10–80 km) from the mainshock epicenter. The El Salvador earthquake occurs at $t = 240.18$ Julian days in 2012 and the Nicoya earthquake occurs at $t = 249.61$ d in Figs. 1–4. We evaluate the prior seismicity in a window 10 d prior to the El Salvador mainshock ($\Delta t_b = 230\text{--}240.18$ d) and the subsequent seismicity from the El Salvador mainshock to the Nicoya mainshock ($\Delta t_a = 240.18\text{--}249.61$ d). The high β values and Z values are consistent with a statistically significant increase in the seismicity rate in the area immediately adjacent to the hypocenter, likely triggered by the El Salvador event. The increase in seismicity after the El Salvador earthquake are clearly shown in Figs. 4c–4d; seismicity rates within a 15 km and 60 km radius from the mainshock epicenter indicate an increase immediately following the El Salvador mainshock.

The seismicity averaged over a number of days may be greatly influenced by this immediate increase in earthquakes within the first few hours after the El Salvador earthquake ($t = 240.18\text{--}241$ d). To remove this contamination, we window the data to exclude the seismicity immediately after the El Salvador mainshock, so that ($\Delta t_a = 241\text{--}249.61$ d). When we take this further measure, the Z values still exceed 2 for all radii, which suggests that the increase in seismicity (relative to the earlier time window) lasted at least a few days following the El Salvador mainshock.

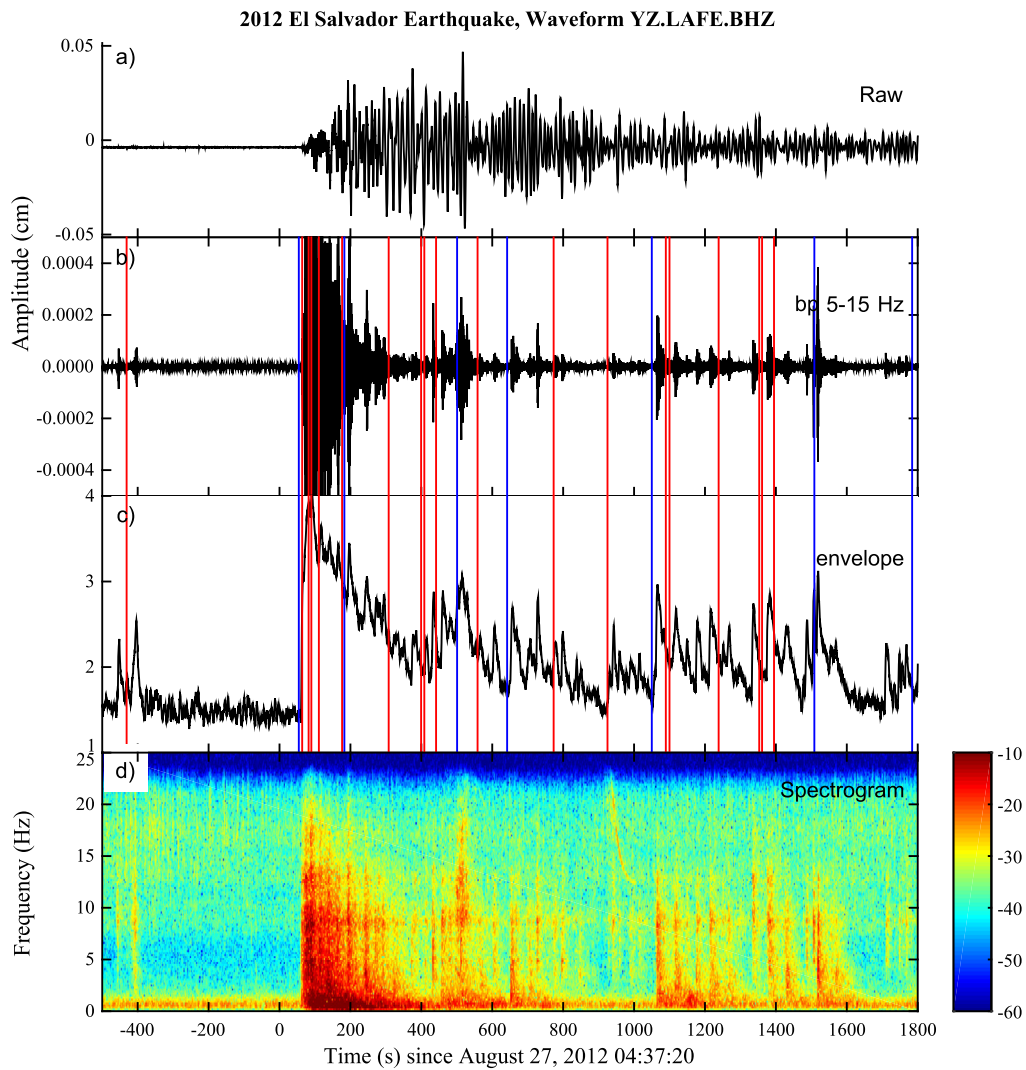


Fig. 3. Local Nicoya Peninsula seismicity triggered by the El Salvador earthquake as recorded at station LAFE. The data is windowed between 500 and 1800 s after the origin time of the El Salvador event and includes (a) instrument-corrected broadband horizontal component of ground velocity, (b) 5–15 Hz frequency band-pass filter of same seismogram, (c) envelope function of the 5–15 Hz filtered seismogram, and (d) spectrogram. Vertical red lines are local seismicity identified by this study, while vertical blue lines are USGS-reported seismicity (<http://earthquake.usgs.gov/earthquakes/map/>) near the El Salvador event, corrected for travel-time to the Nicoya Peninsula. (For interpretation of the references to color in this figure legend, the reader is referred to the web version of this article.)

4.2. Foreshocks and tremor near the mainshock epicenter

Next we compare the seismicity detected in the 9 days prior to the El Salvador earthquake and examine the clustering of events within 0.1 degree bins during that time period (Fig. 4e) with the clustering events in the same bins during the period between the El Salvador and Nicoya earthquakes (Fig. 4f). The greatest density of events shown in Fig. 4f is located directly adjacent to the mainshock epicenter.

Fig. 4f indicates spatial clustering of seismicity between the time periods of the El Salvador and Nicoya mainshocks. When examining the map from Fig. 1 without later aftershocks, clusters of earthquakes and tremor events are shown near the epicenter or beginning of the Nicoya rupture in Fig. 5a. Waveforms of tremor activity are shown in the supplemental material (Fig. S3). While the total tremor depicted in Figs. 1 and 5 is relatively sparse, there are numerous events that occurred adjacent to the mainshock nucleation that were not cataloged due to the strict thresholds described in Section 3.3.

In addition to activity adjacent to the mainshock epicenter, a discrete zone of earthquakes is located updip, near the trench, and along-strike to the southeast of the nucleation point. Also shown

on Fig. 5a is the coseismic slip inversion of continuous and campaign GPS (Protti et al., 2014), indicating that the zone with the most intense earthquake occurrence in the time period between the El Salvador and Nicoya mainshocks is immediately updip of the eventual rupture zone.

The foreshocks also exhibit sustained activity following initial triggering that occurred within the first several hours of the El Salvador mainshock. This continues for the next few days throughout the Nicoya Peninsula (Fig. 5b). Fig. 5c suggests a focusing of earthquake activity, especially within 15 km of the eventual mainshock epicenter in the last ~35 min before the Nicoya mainshock. Protti et al. (2014) reported 3 foreshocks occur in the 35 min prior to the mainshock. Using waveform matching, we detected 6 small foreshocks ($M_L < 2.2$) within ~10 km of the mainshock epicenter (Fig. 5d). Immediate foreshocks are also evident upon comparing Figs. 4c and 4d. Within 15 km of the mainshock epicenter (Fig. 4c), foreshocks immediately precede the mainshock around $t = 249.61$ d with the closer zone displaying a relatively higher concentration of seismicity. In addition, an apparent increase in foreshock activity is shown in the last day before the mainshock (Fig. 5d).

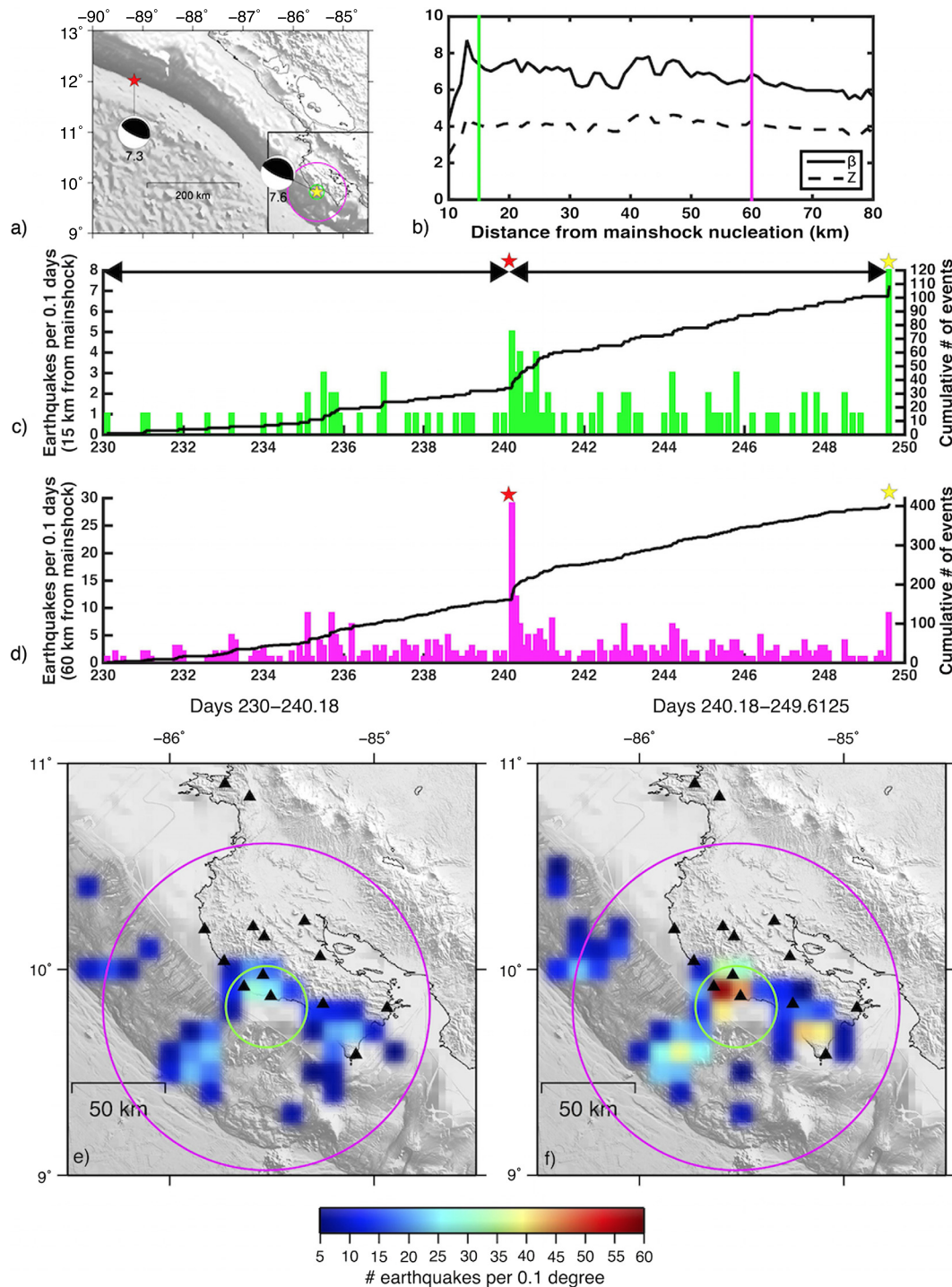


Fig. 4. Evidence of triggering from the El Salvador earthquake near the nucleation of the Nicoya Peninsula earthquake. (a) Map including locations and focal mechanisms (from Global GMT) for the El Salvador and Nicoya earthquakes, showing the significant epicentral distance between the 2 events. (b) β and Z values calculated for a range of radii from the mainshock nucleation point, where green and magenta vertical lines correspond to green and magenta radii in Fig. 1 and other map figures. (c) Seismicity rate for all seismicity within the 15 km of the mainshock nucleation prior to the mainshock timing. (d) Seismicity rate for all seismicity within the 60 km of the mainshock nucleation prior to the mainshock timing. (e) Clustering of earthquake occurrence in bins of 0.1 degrees for the time period day 230–240.18. (f) Clustering of earthquake occurrence in bins of 0.1 degrees for the time period day 240.18–249.6 (right before the mainshock). (For interpretation of the references to color in this figure legend, the reader is referred to the web version of this article.)

To further demonstrate the spatio-temporal evolutions of seismicity, we define 4 time periods around the El Salvador and the Nicoya mainshock (Fig. 6). Between 1 day before the M 7.3 and at the origin time of that earthquake, there is little seismicity throughout the Nicoya Peninsula (Fig. 6a). Immediately after the M 7.3 earthquake, seismicity occurs across the arc, including near the epicenter of the M 7.6 Nicoya Peninsula earthquake, near the

trench directly to the southwest, and in the southern portion of the Peninsula (Fig. 6b). Seismic activity is observed between the period of 1 d after the M 7.3 El Salvador earthquake and 1 d before the M 7.6 Nicoya Peninsula earthquake in the same zones as before (Fig. 6c). In the day prior to the M 7.6 earthquake there are numerous foreshocks in the region immediately adjacent to the mainshock epicenter (Fig. 6d).

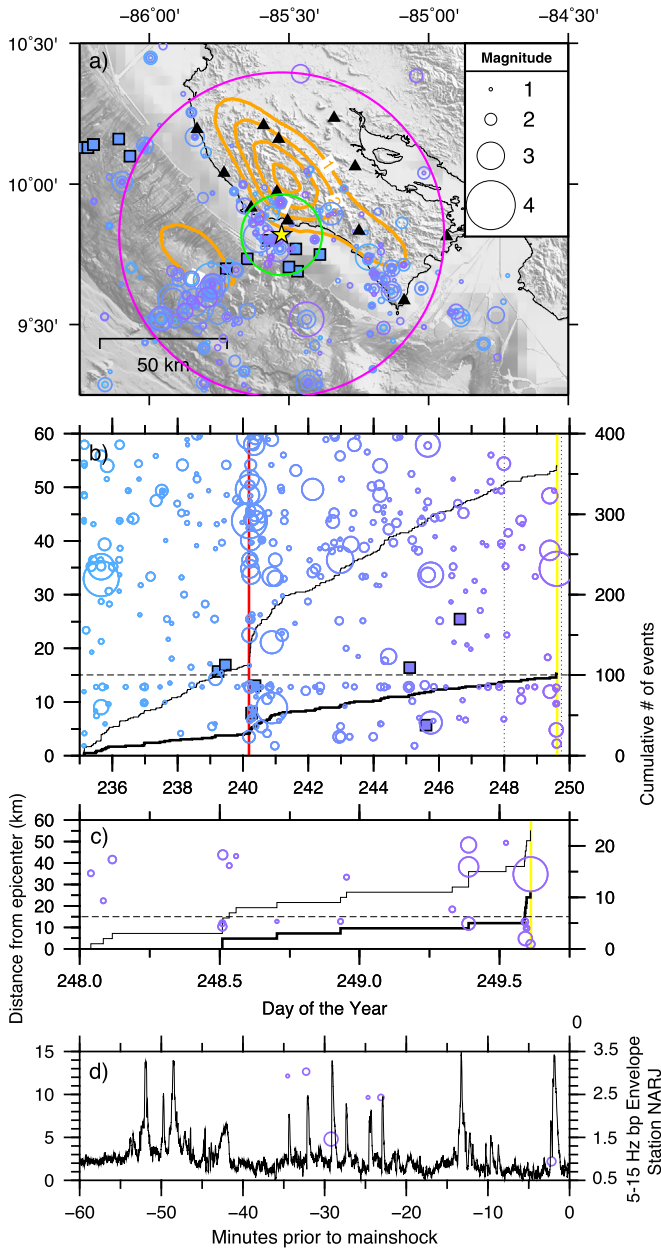


Fig. 5. Spatio-temporal characteristics of foreshocks and tremor. (a) Foreshocks plotted as open circles and tremor as filled squares between day 235 and the Nicoya mainshock. Coseismic slip inversion is shown from Protti et al. (2014) in orange contours. (b) Earthquake and tremor activity as a function of distance and time from the nucleation point. Thin solid and thicker solid stair-step lines indicate cumulative seismic events within 60 and 15 km of the mainshock, respectively. Dashed line at 15 km indicates activity within green circle in Fig. 4a. Vertical dotted line indicates time period for plot in Fig. 4c. (c) Earthquake activity (no tremor occurs during this time period) as a function of distance and time from the nucleation point, within 60 km distance from the nucleation point between days 248–250. Cumulative seismic events plotted as in Fig. 4b. (d) Earthquake activity within 15 km as in (Fig. 4b–c) initiating ~35 min prior to the mainshock. Also shown is the envelope of ground velocity amplitude at station NARJ (the closest operating station to the epicenter) indicating seismic activity corresponding to the earthquakes within 15 km, as well as other activity that may be local earthquakes or tremor elsewhere in the Nicoya Peninsula.

5. Discussion

5.1. Spatio-temporal patterns of the pre-Nicoya mainshock seismicity

Generally, earthquake behavior appears highly clustered with no fundamental differences in spatio-temporal distribution be-

tween foreshocks and aftershocks (e.g. Brodsky, 2011). It is only “after the fact” that we assign foreshock and aftershock categories. Thus, determining the robustness of seismicity rate changes in a region is a common hurdle for potential earthquake forecasting. Waveform matching offers the ability for developing increased and systematic earthquake detections, leading to more robust earthquake catalogs with reduced magnitudes of completeness. While the method only detects earthquakes in regions near template events, which may bias the results, it provides a useful tool for better understanding seismicity by effectively improving the detection threshold.

In the absence of other corroborating information such as high precision nearby geodetic data, seismicity offers a glimpse into preparatory processes prior to earthquakes. The Tohoku–Oki event was preceded by a prolonged sequence of migrating activity (Kato et al., 2012). Those earthquakes migrated 10s of kilometers over weeks, with a quiescent period of ~9 days prior to the Tohoku–Oki mainshock. In this study, we focus on the discrete zone around the mainshock epicenter as its proximity has plausible implications for initiating rupture of the mainshock (green circle in Figs. 1, 4, and 5). This activity appears to have been triggered by the far-field El Salvador earthquake, which occurred 9 days prior to the Nicoya mainshock. The increase in activity is manifested as a statistically significant increase in seismicity right around the timing of the El Salvador earthquake (Fig. 3).

The geologic context provided by past scientific studies indicates the zone that ruptured in the Nicoya earthquake was identified as a clearly coupled patch, as indicated by geodetic measurements in the last decade (Feng et al., 2012; Protti et al., 2014), surrounded by a weakly coupled patch, that was also identifiable through a change in mapped earthquake b-values (Ghosh et al., 2008). To the west of the mainshock nucleation zone and the cluster of vigorous aftershock activity is a zone undergoing slow slip and tremor (Walter et al., 2011) as well as intermittent very low-frequency earthquakes (Walter et al., 2013). The plate interface exists at a depth of ~10–20 km here (Kyriakopoulos et al., 2015). To the east of the mainshock and adjacent to the Nicoya Gulf exists an area that has experienced the greatest quantity and magnitude of slow slip events at the Nicoya Peninsula (Outerbridge et al., 2010; Jiang et al., 2012; Dixon et al., 2014) at a plate interface depth of ~30–40 km.

Though the coseismic rupture area was previously identified as a strongly coupled region, we find evidence for distant triggering by the El Salvador earthquake within this zone (Figs. 4f, 5, and 6b). Approximately 9 days later, the mainshock began to slip near the immediate foreshock concentration (Figs. 5d and 6d) and then dynamically ruptured in the downdip direction (Yue et al., 2013) with termination at the Mohorovičić discontinuity. After the event the majority of the early aftershocks locate near the updip extent of the coseismic rupture (Protti et al., 2014). Clustering of seismicity at this zone suggests that the plate interface may be considerably weaker there, due to its susceptibility to triggering (Brodsky and van der Elst, 2014). Brodsky and Lay (2014) documented an earthquake sequence in Chile, adjacent to a geodetically locked patch, culminated in megathrust rupture, whereas other swarms do not. The Nicoya Peninsula appears to be another case where an increase in the seismicity rate adjacent to or within a locked patch culminates in a megathrust rupture.

Although many high-frequency signals are detected after the El Salvador, there are still some similar signals that are not matched by local templates (Fig. 3). This may be caused by incompleteness of the template waveforms and/or contamination from the El Salvador mainshock and large aftershocks. Due to the large source-receiver distance of many templates and possible contamination from El Salvador rupture zone, many initial detections have relatively low cross-correlation coefficients (Fig. S4a). Hence, it is

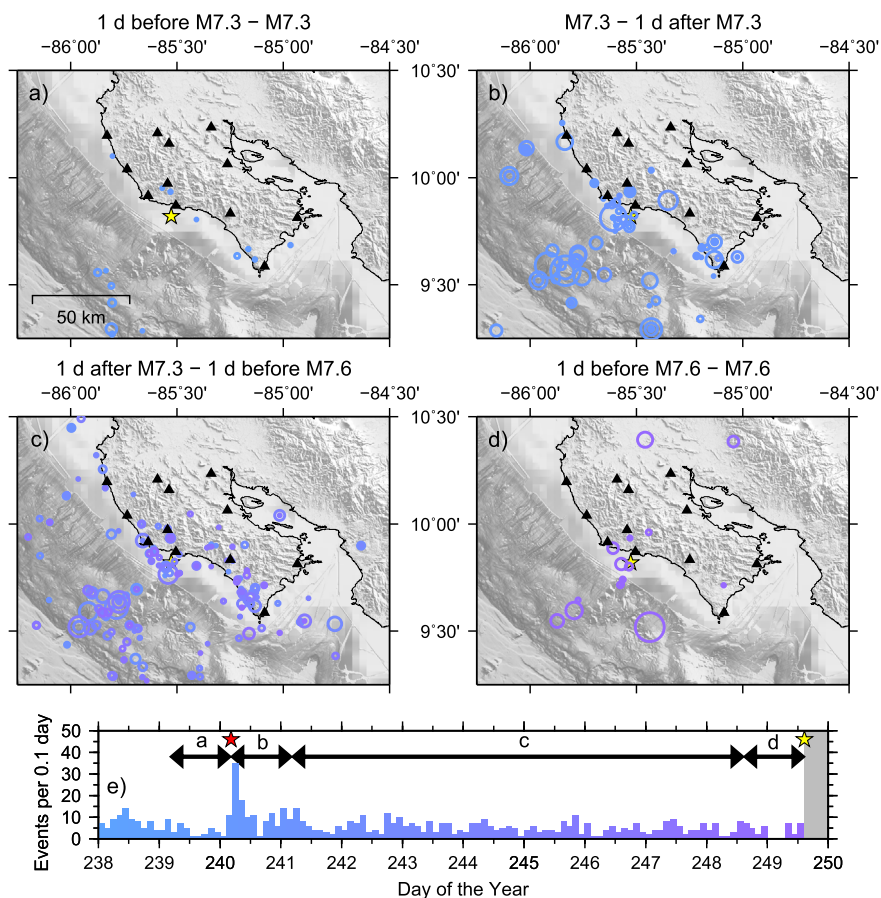


Fig. 6. Spatio-temporal characteristics of foreshock sequences. (a) Seismic activity within one day before the origin time of the M_W 7.3 El Salvador mainshock. (b) Seismic activity within one day after the El Salvador mainshock. (c) Seismic activity from 1 d after the El Salvador mainshock through 1 d before the M_W 7.6 Nicoya mainshock. (d) Seismic activity within the last day before the origin time of the Nicoya seismicity, showing the immediate foreshocks. (e) Seismicity rate, as in Fig. 1d, with the time periods in (a–d) marked.

necessary to investigate the dependence of the results on study parameters in Section 3.1. The β values remain high enough to indicate statistical significance, even if the MAD threshold for detection is raised so that only higher-quality matches are included (Fig. S5). Similarly, we compute β values with different cutoff-magnitude and cutoff cross-correlation coefficient, and/or immediate foreshocks are excluded (Fig. S4). The significant increase of seismicity after the El Salvador mainshock is still evident. For cutoff-magnitude smaller than M_C , our detections show a significant decrease in seismicity. The seismicity rate decrease of very small earthquakes can be best explained by the contamination from the El Salvador sequences, which effectively impede detection of very small events. In summary, although our method still misses some events, especially immediately following the El Salvador mainshock, the general observation of a clear increase in seismicity near Nicoya Peninsula following the distant mainshock remains robust.

The observed seismic activity itself could be diagnostic of one of two foreshock models (Mignan, 2014): the *pre-slip* or the *earthquake cascade model*. Clear migrating foreshocks were observed immediately before the 2011 Tohoku–Oki earthquake (Kato et al., 2012), supporting the inference of a propagating slow-slip. However, we did not observe any clear migration of foreshocks immediately before the Nicoya Peninsula mainshock. In addition, while slow-slip events occurred in May 2012 (Dixon et al., 2014; Malservisi et al., 2015), there was no clear GPS evidence of slow-slip events in the last 9 days right before the mainshock. Hence, we cannot conclude definitely that they were driven by slow-slip related to mainshock nucleation over the course of multiple days.

Another potential issue is that in this study we simply assign the location of the template event to the detected event. In reality, their locations could be different and may not reveal migration of the events.

5.2. Statistical significance test of remotely triggered seismicity

The sustained increase in seismicity rate over the first day after the El Salvador event (Figs. 4, 6b) and continuing for the next day or so (Fig. 6c) suggests a process driving seismicity over a longer duration than simple dynamic triggering during the surface waves. The exact cause of a high seismicity rate long after surface waves is currently under debate. Possible mechanisms include secondary aftershocks (Brodsky, 2006), fault weakening (Parsons, 2005), and triggered stress transients (Shelly et al., 2011). In order to assess whether the observed seismicity in the 9 days between events is driven by some external forces instead of simply earthquake interactions (i.e. aftershocks of those initially triggered events), we apply an Epidemic Type Aftershock Sequence (ETAS) model and determine whether our observations deviate from that model. In the ETAS model (Ogata, 1988), the seismicity rate at time t is described as

$$R(t) = \mu + \sum_{t_i \leq t} \frac{K e^{\alpha(M_i - M_C)}}{(t - t_i + c)^p}$$

where μ is the background seismicity rate, c and p are Omori's law parameters, K is the aftershock productivity, α reflects how efficient a certain magnitude earthquake generates aftershocks, t_i is

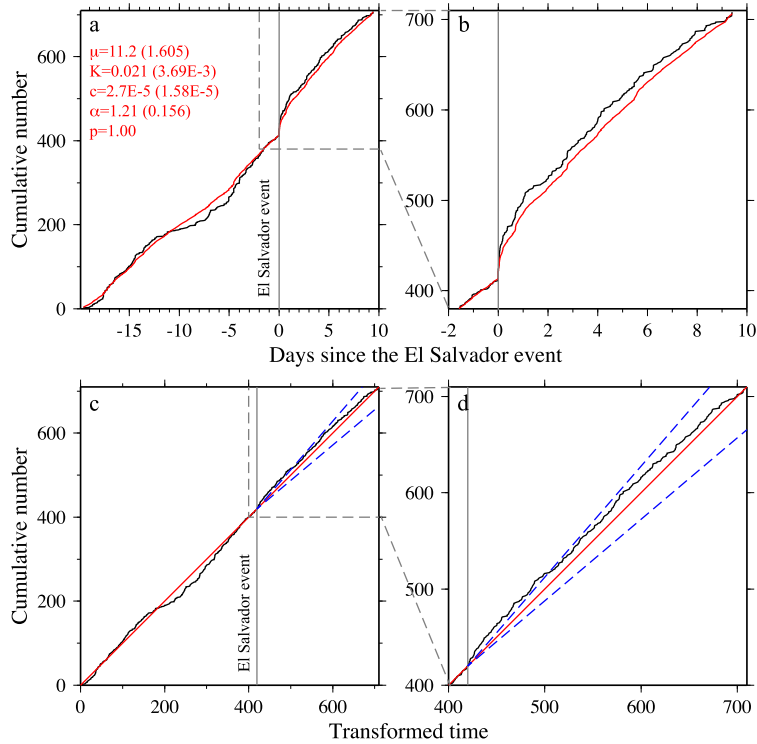


Fig. 7. Epidemic-type aftershock sequence (ETAS) model for the Nicoya Peninsula seismicity. (a) Cumulative number of events versus time. Black and red curves denote the observed number and ETAS modeling, respectively. The optimal fitting parameters are shown in red. The standard error of each parameter is shown in brackets. (b) Zoom-in plot of the dashed box in (a). (c) Cumulative number of events versus transformed time. Black and red curves denote the observed number and ETAS modeling, respectively. (d) Zoom-in plot of the dashed box in (c). Blue dash lines denote two times standard deviation of ETAS prediction. (For interpretation of the references to color in this figure legend, the reader is referred to the web version of this article.)

the origin time of the i -th earthquake. We first fit the background seismicity 20 days before the El Salvador event and obtain optimal parameters by maximum likelihood estimation using software SASeis2006 (Ogata, 2006) (Figs. 7a and 7b). We have to fix $p = 1$ in order to get stable fitting parameters. We predict the seismicity rate changes after the El Salvador event using those optimal parameters. Upon first inspection, the prediction clearly underestimates the seismicity rate after the El Salvador mainshock (Fig. 7b).

We conduct standard error analysis on the ETAS parameters by simulation, which is a more accurate approach than the Hessian matrix analysis (Wang et al., 2010; Bansal and Ogata, 2013). Following (Wang et al., 2010), we obtain the standard errors of the ETAS parameters by simulating 2000 earthquake catalogs using the software package PtProcess (Harte, 2010) with the previously obtained parameters. For each simulation, the ETAS parameters are obtained from the simulated earthquake catalog. The standard error can then be defined as follows:

$$\sqrt{\frac{\sum_{i=1}^{2000} (\text{parameter estimated from simulated catalog} - \text{true value})^2}{2000}}$$

To better quantify the deviation between the observed number of events and prediction, we compute theoretical number of events (i.e., transformed time τ_i). The transformed time is calculated as:

$$\tau_i = \int_0^{t_i} R(s) ds$$

where R is the predicted seismicity rate by the ETAS model, t_i is the origin time of the i th event in the catalog, s is the origin time of earthquakes prior to t_i . When a catalog can be well described by the same set of parameters, we expect to see well-fitted cumulative number of events throughout the whole study period (Ogata,

2005; Llenos et al., 2009). However, we find clear misfit immediately after the El Salvador mainshock. To evaluate whether the misfit can be explained as random fluctuations in parameters, we compute the two times standard deviation of the expected number from ETAS prediction, following Ogata (1988) and Llenos et al. (2009). Fig. 7d illustrates that, at the onset of the seismicity rate increase, it clearly exceeds two times standard deviation of the ETAS prediction, which affirms the statistical significance of the misfit. The significant deviation indicates that the high seismicity after the El Salvador event cannot be simply explained as secondary aftershocks alone. Instead, the dynamic stress changes from the El Salvador mainshock may trigger stress transients or weaken the fault system near Nicoya for at least the few days after the El Salvador event. In another study, a misfit in observed seismicity compared to an ETAS prediction for a seismic swarm at a transform fault near the Galapagos Islands led to the conclusion that the swarm was plausibly driven by other triggering phenomena than the ETAS model of seismic events triggering other seismic events (Roland and McGuire, 2009). It is possible that other stress transients, such as slow slip or fluid flow (Vidale and Shearer, 2006; Lohman and McGuire, 2007) drive this type of behavior.

5.3. Possible slow slip or other transients?

There are a few additional factors that suggest slow slip or other stress transients could have driven the foreshocks. We did observe a clear increase of microseismicity further offshore, near the Nicoya trench immediately after the El Salvador earthquake. In addition, the foreshocks showed a sudden increase in the last day leading to the mainshock (Fig. 6d), somewhat similar to the case observed right before the 1999 Izmit earthquake (Bouchon et al., 2011). Finally, after negligible tremor detected earlier in 2012 (Fig. S6), we identified an increase in tremor activity located within a 20-km radius of the 2012 Nicoya mainshock starting ~10 days

before its occurrence (Fig. 5b). After a few days of quiescence, tremor continues 4 days before the mainshock. Although only a few tremor episodes are plotted within this time period, a significant increase in tremor activity was visually documented (Fig. S3) that could not be successfully located. Such increase of tremor activity may have been triggered by slow slip on the plate interface.

Hence, it is plausible that slow slip may occur both in the epicenter and offshore as a result of delayed dynamic triggering (Shelly et al., 2011), but was too small to be observed geodetically. Interestingly, Peng et al. (2015) found that the 2004 M_w 6.0 South Napa earthquake triggered a major tremor episode that lasted for more than 3 weeks at the Parkfield–Cholame section of the San Andreas Fault (at a distance of more than 200 km). In this case, intensive tremor started about 12 h after the South Napa mainshock, and showed systematic along-strike migration, suggesting that they are driven by slow slip remotely triggered by the South Napa mainshock, although the slow slip was not observed even with sensitive borehole strainmeters.

Finally, Kato et al. (2012) and Kato and Nakagawa (2014) have identified many repeating earthquakes in the foreshock sequences of the 2011 Tohoku–Oki and 2014 Iquique earthquakes, and used them to infer aseismic slip along the plate boundaries. Our preliminary results also found some repeating earthquakes before the Nicoya mainshock (Yao et al., 2014). However, they are much less prevalent compared with repeating events after the mainshock. Further analysis is needed to better quantify their existence and relationship with possible aseismic slip in our study region.

6. Conclusions

Using a waveform matched-filter technique to augment the seismicity catalog, we found that the El Salvador earthquake, which ruptured 9 days before and 450 km to the northwest of the Nicoya earthquake, had triggered an immediate increase of local seismicity near Nicoya. This activity was sustained for only a few days. Prior to the Nicoya mainshock, some small events occurred in this same area immediately updip of the Nicoya hypocenter ~35 min prior to its rupture. This type of immediate foreshock behavior indicates possible delayed dynamic triggering of a slow-slip event that could have initiated the Nicoya Peninsula mainshock. However, we were unable to observe any geodetic evidence of such slow-slip event do to a lack of offshore geodesy here.

The results indicate that earthquakes at regional distances may trigger one-another by delayed dynamic triggering (Shelly et al., 2011; Peng et al., 2015). If true, this suggests that real-time monitoring may be useful in detecting such changes. However, it is not clear yet, how much more likely a large earthquake is to rupture during such triggered shallow slow-slip. The density of station spacing in the Nicoya Peninsula is considerably higher than most regions along the Central American arc. Even with this improved data availability, during routine operations, the increase in seismicity near Nicoya following the El Salvador event would likely not have been noticed by even the most skilled analysts. Thus, seismological methods would need to improve significantly with semi-automatic detection/location systems in order to identify potential changes in seismicity rates. Finally, as highlighted by Newman (2011), it would also be of great benefit to have sensitive geodetic time series data offshore, to aid in detecting and quantifying precursory slow-slip and other aseismic creep events.

Acknowledgements

We thank Victor Gonzalez for his help constructing and operating the Nicoya seismic and continuous GPS network and Stephanie Taylor for preliminary Nicoya tremor detections. This work was supported by National Science Foundation grants NSF-0847382,

NSF-1262267 to AVN, and NSF-1321552 to ZP and AVN. NSF EAR-1321550 to SYS also funded this work. We used the Keeneland GPU cluster in the Extreme Science and Engineering Discovery Environment (XSEDE), which is supported by National Science Foundation grant number OCI-1053575. Some seismic instruments used in the field program were provided by the PASSCAL facility of the Incorporated Research Institutions for Seismology (IRIS) through the PASSCAL Instrument Center at New Mexico Tech. Seismic data collected during this experiment is available through the IRIS Data Management Center. The facilities of the IRIS Consortium are supported by the National Science Foundation under Cooperative Agreement EAR-0552316 and by the Department of Energy National Nuclear Security Administration. Some figures were created using Generic Mapping Tools (Wessel et al., 2013). We thank two anonymous reviewers and editor Peter Shearer for their comments that improved this manuscript.

Appendix A. Supplementary material

Supplementary material related to this article can be found online at <http://dx.doi.org/10.1016/j.epsl.2015.09.017>.

References

- Ampuero, J.-P., Rubin, A.M., 2008. Earthquake nucleation on rate and state faults – aging and slip laws. *J. Geophys. Res.* 113, B01302. <http://dx.doi.org/10.1029/2007JB005082>.
- Bansal, A.R., Ogata, Y., 2013. A non-stationary epidemic type aftershock sequence model for seismicity prior to the December 26, 2004 M 9.1 Sumatra–Andaman Islands mega-earthquake. *J. Geophys. Res., Solid Earth* 118, 616–629. <http://dx.doi.org/10.1002/jgrb.50068>.
- Borrero, J.C., Kalligeris, N., Lynett, P.J., Fritz, H.M., Newman, A.V., Convers, J.A., 2014. Observations and modelling of the August 27, 2012 earthquake and tsunami affecting El Salvador and Nicaragua. *Pure Appl. Geophys.* 171 (12), 3421–3435. <http://dx.doi.org/10.1007/s00024-014-0782-2>.
- Bouchon, M., Karabulut, H., Aktar, M., Özalaybey, S., Schmittbuhl, J., Bouin, M.-P., 2011. Extended nucleation of the 1999 M_w 7.6 Izmit earthquake. *Science* 331, 877–880. <http://dx.doi.org/10.1126/science.1197341>.
- Bouchon, M., Durand, V., Marsan, D., Karabulut, H., Schmittbuhl, J., 2013. The long precursory phase of most large interplate earthquakes. *Nat. Geosci.* 6, 1769–1785.
- Brodsky, E.E., 2006. Long-range triggered earthquakes that continue after the wave train passes. *Geophys. Res. Lett.* 33 (15).
- Brodsky, E.E., 2011. The spatial density of foreshocks. *Geophys. Res. Lett.* 38, L10305. <http://dx.doi.org/10.1029/2011GL047253>.
- Brodsky, E.E., Lay, T., 2014. Recognizing foreshocks from the 1 April 2014 Chile earthquake. *Science* 344, 200. <http://dx.doi.org/10.1126/science.1255202>.
- Brodsky, E.E., Van der Elst, N.J., 2014. The uses of dynamic earthquake triggering. *Annu. Rev. Earth Planet. Sci.* 42, 317–339. <http://dx.doi.org/10.1146/annurev-earth-060313-054648>.
- Brown, J.R., Beroza, G.C., Shelly, D.R., 2008. An autocorrelation method to detect low frequency earthquakes within tremor. *Geophys. Res. Lett.* 35, L16305. <http://dx.doi.org/10.1029/2008GL034560>.
- DeMets, C., Gordon, R.G., Argus, D.F., 2010. Geologically current plate motions. *Geophys. J. Int.* 181, 1–80. <http://dx.doi.org/10.1111/j.1365-246X.2009.04491.x>.
- DeShon, H.R., Schwartz, S.Y., Newman, A.V., Gonzalez, V., Protti, J.M., Dorman, L.M., Dixon, T., Norabuena, E., Flueh, E., 2006. Seismogenic zone structure beneath the Nicoya Peninsula, Costa Rica, from 3D local earthquake P and S wave tomography. *Geophys. J. Int.* 164, 109–124. <http://dx.doi.org/10.1111/j.1365-246X.2005.02809.x>.
- Dieterich, J.H., 1979. Modeling of rock friction: 1. Experimental results and constitutive equations. *J. Geophys. Res.* 84, 2161–2168. <http://dx.doi.org/10.1029/JB084iB05p02161>.
- Dixon, T., Jiang, Y., Malservisi, R., McCaffrey, R., Voss, N., Protti, M., Gonzalez, V., 2014. Earthquake and tsunami forecasts: relation of slow slip events to subsequent earthquake rupture. *Proc. Natl. Acad. Sci.* <http://dx.doi.org/10.1073/pnas.1412299111>.
- Dodge, D.A., Beroza, G.C., Ellsworth, W.L., 1995. Foreshock sequence of the 1992 landers, California, earthquake and its implications for earthquake nucleation. *J. Geophys. Res.* 100, 9865–9880.
- Doi, I., Kawakata, H., 2012. A non-accelerating foreshock sequence followed by a short period of quiescence for a large inland earthquake. *Geophys. Res. Lett.* 39, L11308. <http://dx.doi.org/10.1029/2012GL051779>.
- Felzer, K.R., Abercrombie, R.E., Ekström, G., 2004. A common origin for aftershocks, foreshocks and multiplets. *Bull. Seismol. Soc. Am.* 94, 88–98.

- Felzer, K.R., Page, M.T., Michael, A.J., 2015. Artificial seismic acceleration. *Nat. Geosci.* 8, 82–83.
- Feng, L., Newman, A.V., Protti, J.M., González, V., Jiang, Y., Dixon, T.H., 2012. Active deformation near the Nicoya Peninsula, Northwestern Costa Rica, between 1996 and 2010: interseismic megathrust coupling. *J. Geophys. Res.* 117, B06407. <http://dx.doi.org/10.1029/2012JB009230>.
- Ghosh, A., Newman, A.V., Thomas, A.M., Farmer, G.T., 2008. Interface locking along the subduction megathrust from microseismicity near Nicoya, Costa Rica. *Geophys. Res. Lett.* 35 (L01301). <http://dx.doi.org/10.1029/2007GL031617>.
- Habermann, R.E., 1981. Precursory seismicity patterns: stalking the mature seismic gap. In: Simpson, D.W., Richards, P.G. (Eds.), *Earthquake Prediction – An International Review*. American Geophysical Union, pp. 29–42.
- Harte, D., 2010. PtProcess: an R package for modeling marked point process indexed by time. *J. Stat. Softw.* 35 (8), 1–32.
- Helmstetter, A., Sornette, D., Grasso, J.-R., 2003. Mainshocks are aftershocks of conditional foreshocks: how do foreshock statistical properties emerge from aftershock laws. *J. Geophys. Res.* 108 (B1), 2046. <http://dx.doi.org/10.1029/2002JB001991>.
- Hill, D.P., Prejean, S., 2007. Dynamic triggering. In: Kanamori, H. (Ed.), *Earthquake Seismology*. In: *Treatise on Geophysics*. Elsevier, Amsterdam, pp. 257–291 (G. Schubert, ed. in Chief).
- Holtkamp, S.G., Pritchard, M.E., Lohman, R.B., 2011. Earthquake swarms in South America. *Geophys. J. Int.* 187, 128–146. <http://dx.doi.org/10.1111/j.1365-246X.2011.05137.x>.
- Ito, Y., Hino, R., Kido, M., Fujimoto, H., Osada, Y., Inazu, D., Ohta, Y., Iinuma, T., Ohzono, M., Miura, S., Mishina, M., Suzuki, K., Tsuji, T., Ashi, J., 2013. Episodic slow slip events in the Japan subduction zone before the 2011 Tohoku–Oki earthquake. *Tectonophysics* 600, 14–26.
- Jiang, Y., Wdowinski, S., Dixon, T.H., Hackl, M., Protti, M., Gonzalez, V., 2012. Slow slip events in Costa Rica detected by continuous GPS observations, 2002–2011. *Geochem. Geophys. Geosyst.* 13, Q04006.
- Jones, L.M., Molnar, P., 1979. Some characteristics of foreshocks and their possible relationship to earthquake prediction and premonitory slip on faults. *J. Geophys. Res.* 84 (B7), 3596–3608. <http://dx.doi.org/10.1029/JB084iB07p03596>.
- Kanamori, H., 1972. Mechanism of tsunami earthquakes. *Phys. Earth Planet. Inter.* 6, 346–359.
- Kato, A., Obara, K., Igarashi, T., Tsuruoka, H., Nakagawa, S., Hirata, N., 2012. Propagation of slow slip leading up to the 2011 M_w 9.0 Tohoku–Oki earthquake. *Science*. <http://dx.doi.org/10.1126/science.1215141>.
- Kato, A., Nakagawa, S., 2014. Multiple slow-slip events during a foreshock sequence of the 2014 Iquique, Chile M_w 8.1 earthquake. *Geophys. Res. Lett.* 41, 5420–5427. <http://dx.doi.org/10.1002/2014GL061138>.
- Kyriakopoulos, C., Newman, A.V., Thomas, A.M., Moore-Driskell, M., Farmer, G.T., 2015. A new seismically constrained subduction interface model for Central America. *J. Geophys. Res.* 120. <http://dx.doi.org/10.1002/2014JB011859>.
- Lengliné, O., Marsan, D., 2009. Inferring the coseismic and postseismic stress changes caused by the 2004 M_w = 6 Parkfield earthquake from variations of recurrence times of microearthquakes. *J. Geophys. Res.* 114, B10303. <http://dx.doi.org/10.1029/2008JB006118>.
- Lengliné, O., Enescu, B., Peng, Z., Shiomi, K., 2012. Decay and expansion of the early aftershock activity following the 2011, M_w 9.0 Tohoku earthquake. *Geophys. Res. Lett.* 39, L18309. <http://dx.doi.org/10.1029/2012GL052797>.
- Llenos, A.L., McGuire, J.J., Ogata, Y., 2009. Modeling seismic swarms triggered by aseismic transients. *Earth Planet. Sci. Lett.* 281 (1–2), 59–69.
- Lohman, R.B., McGuire, J.J., 2007. Earthquake swarms driven by aseismic creep in the Salton Trough, California. *J. Geophys. Res., Solid Earth* 112 (B4).
- Malservisi, R., Schwartz, S.Y., Voss, N., Protti, M., Gonzalez, V., Dixon, T.H., Jian, Y., Newman, A.V., Walter, J.J., Vayenko, D., 2015. Multiscale postseismic behavior on a megathrust: the 2012 Nicoya earthquake, Costa Rica. *Geochem. Geophys. Geosyst.* 16, 1–17. <http://dx.doi.org/10.1002/2015GC005794>.
- Marsan, D., Wyss, M., 2011. Seismicity rate changes. Community Online Resource for Statistical Seismicity Analysis, <http://dx.doi.org/10.5078/corssa-25837590>. Available at <http://www.corssa.org>.
- Marshall, J.S., Anderson, R.S., 1995. Quaternary uplift and seismic cycle deformation, Peninsula de Nicoya, Costa Rica. *Geol. Soc. Am. Bull.* 107 (4), 463–473. <http://dx.doi.org/10.1130/0016-7606>.
- Matthews, M.V., Reasenber, P.A., 1988. Statistical methods for investigating quiescence and other temporal seismicity patterns. *Pageoph* 126, 357–372.
- McGuire, J.J., Boettcher, M., Jordan, T.H., 2005. Foreshock sequences and earthquake predictability on East Pacific rise transform faults. *Nature* 434, 457–461.
- Meng, X., Yu, X., Peng, Z., Hong, B., 2012. Detecting earthquakes around Salton Sea following the 2010 M_w 7.2 El Mayor-Cucapah earthquake using GPU parallel computing. *Proc. Comput. Sci.* 9, 937–946. <http://dx.doi.org/10.1016/j.procs.2012.04.100>.
- Meng, X., Peng, Z., Hardebeck, J., 2013. Seismicity around Parkfield correlates with static shear stress changes following the 2003 M_w 6.5 San Simeon earthquake. *J. Geophys. Res.* 118 (7), 3576–3591. <http://dx.doi.org/10.1002/jgrb.50271>.
- Meng, X., Peng, Z., in press. Seismicity rate changes in the San Jacinto fault zone and the Salton Sea geothermal field following the 2010 M_w 7.2 El Mayor-Cucapah earthquake. *Geophys. J. Int.* <http://dx.doi.org/10.1093/gji/ggu085>.
- Mignan, A., 2014. The debate on the prognostic value of earthquake foreshocks: a meta-analysis. *Sci. Rep.* 4, 4099. <http://dx.doi.org/10.1038/srep04099>.
- Mogi, K., 1963. Some discussions on aftershocks, foreshocks and earthquake swarms – the fracture of a semi-infinite body caused by an inner stress origin and its relation to the earthquake phenomena. *Bull. Earthq. Res. Inst. Univ. Tokyo* 41, 615–658. Third paper.
- Moore-Driskell, M., DeShon, H.R., Rabbel, W., Thorwart, M., Dzierma, Y., Arroyo, I.G., 2013. Integration of arrival-time datasets for consistent quality control: a case study of amphibious experiments along the middle America trench. *Bull. Seismol. Soc. Am.* 103 (5), 2752–2766. <http://dx.doi.org/10.1785/0120120274>.
- Newman, A.V., 2011. Hidden depths. *Nature* 474, 441–443. <http://dx.doi.org/10.1038/474441a>.
- Nishenko, S.P., 1991. Circum-Pacific seismic potential: 1989–1999. *Pure Appl. Geophys.* 135 (2), 169–259. <http://dx.doi.org/10.1007/BF00880240>.
- Ogata, Y., 1988. Statistical-models for earthquake occurrences and residual analysis for point-processes. *J. Am. Stat. Assoc.* 83 (401), 9–27.
- Ogata, Y., 2005. Detection of anomalous seismicity as a stress change sensor. *J. Geophys. Res., Solid Earth* 110 (B5).
- Ogata, Y., 2006. Fortran programs statistical analysis of seismicity – updated version (point process data). EPTREN, LINLIN, SIMBVP, LINSIM and PGRAPH included in Time Series and Control Program Package, SASeis2006. In: *Computer Science Monograph*, No. 33.
- Outerbridge, K.C., Dixon, T.H., Schwartz, S.Y., Walter, J.J., Protti, M., Gonzalez, V., Biggs, J., Thorwart, M., Rabbel, W., 2010. A tremor and slip event on the Cocos-Caribbean subduction zone as measured by a GPS and seismic network on the Nicoya Peninsula, Costa Rica. *J. Geophys. Res.* 115, B10408. <http://dx.doi.org/10.1029/2009JB006845>.
- Parsons, T., 2005. A hypothesis for delayed dynamic earthquake triggering. *Geophys. Res. Lett.* 32 (4).
- Peng, Z., Zhao, P., 2009. Migration of early aftershocks following the 2004 Parkfield earthquake. *Nat. Geosci.* 2, 877–881. <http://dx.doi.org/10.1038/ngeo697>.
- Peng, Z., Shelly, D.R., Ellsworth, W., 2015. Delay dynamic triggering of deep tremor along the Parkfield-Cholame section of the San Andreas Fault following the 2014 $M_6.0$ South Napa earthquake. *Geophys. Res. Lett.* <http://dx.doi.org/10.1002/2015GL065277>.
- Protti, M., et al., 1995. The March 25, 1990 (M_w = 7.0, M_L = 6.8), earthquake at the entrance of the Nicoya Gulf, Costa Rica: its prior activity, foreshocks, aftershocks, and triggered seismicity. *J. Geophys. Res.* 100 (B10), 20345–20358. <http://dx.doi.org/10.1029/94JB03099>.
- Protti, M., Güendel, M.F., Malavassi, E., 2001. *Evaluación del Potencial Sísmico de la Península de Nicoya*, 1st edn. Editorial Fundación Universidad Nacional, Heredia, Costa Rica. 144 pp.
- Protti, M., González, V., Newman, A.V., Dixon, T.H., Schwartz, S.Y., Marshall, J.S., Feng, L., Walter, J.J., Malservisi, R., Owen, S.E., 2014. Nicoya earthquake rupture anticipated by GPS measurements of the locked plate interface. *Nat. Geosci.* 7 (2), 117–121. <http://dx.doi.org/10.1038/ngeo2038>.
- Roeloffs, E.A., 2006. Evidence for aseismic deformation rate changes prior to earthquakes. *Annu. Rev. Earth Planet. Sci.* 34, 591–627.
- Roland, E., McGuire, J.J., 2009. Earthquake swarms on transform faults. *Geophys. J. Int.* 178 (3), 1677–1690.
- Satake, K., 1994. Mechanism of the 1992 Nicaragua tsunami earthquake. *Geophys. Res. Lett.* 21, 2519–2522. <http://dx.doi.org/10.1029/94GL02338>.
- Schaff, D.P., Waldhauser, F., 2010. One magnitude unit reduction in detection threshold by cross correlation applied to Parkfield (California) and China seismicity. *Bull. Seismol. Soc. Am.* 100 (6), 3224–3238.
- Shearer, P.M., 1994. Global seismic event detection using a matched filter on long-period seismograms. *J. Geophys. Res.* 99, 13,713–13,725.
- Shelly, D.R., Beroza, G.C., Ide, S., 2007. Complex evolution of transient slip derived from precise tremor locations in western Shikoku, Japan. *Geochem. Geophys. Geosyst.* 8, Q10014. <http://dx.doi.org/10.1029/2007GC001640>.
- Shelly, D.R., Hardebeck, J.L., 2010. Precise tremor source locations and amplitude variations along the lower-crustal central San Andreas Fault. *Geophys. Res. Lett.* 37, L14301. <http://dx.doi.org/10.1029/2010GL043672>.
- Shelly, D.R., Hill, D.P., 2011. Migrating swarms of brittle-failure earthquakes in the lower crust beneath Mammoth Mountain California. *Geophys. Res. Lett.* 38, L20307. <http://dx.doi.org/10.1029/2011GL049336>.
- Shelly, D.R., Peng, Z., Hill, D.P., Aiken, C., 2011. Triggered creep as a possible mechanism for delayed dynamic triggering of tremor and earthquakes. *Nat. Geosci.* 4, 384–388. <http://dx.doi.org/10.1038/ngeo1141>.
- Vidale, J.E., Shearer, P.M., 2006. A survey of 71 earthquake bursts across southern

- California: exploring the role of pore fluid pressure fluctuations and aseismic slip as drivers. *J. Geophys. Res.* 111, B05312. <http://dx.doi.org/10.1029/2005JB004034>.
- Walter, J.I., Schwartz, S.Y., Protti, J.M., Gonzalez, V., 2011. Persistent tremor within the northern Costa Rica seismogenic zone. *Geophys. Res. Lett.* 38, L01307. <http://dx.doi.org/10.1029/2010GL045586>.
- Walter, J.I., Schwartz, S.Y., Protti, M., Gonzalez, V., 2013. The synchronous occurrence of shallow tremor and very low frequency earthquakes offshore of the Nicoya Peninsula, Costa Rica. *Geophys. Res. Lett.* 40, 1517–1522. <http://dx.doi.org/10.1002/grl.50213>.
- Wang, Q., Schoenberg, F.P., Jackson, D.D., 2010. Standard errors of parameter estimates in the ETAS model. *Bull. Seismol. Soc. Am.* 100 (5A), 1989–2001.
- Wech, A.G., Creager, K.C., 2008. Automated detection and location of Cascadia tremor. *Geophys. Res. Lett.* 35 (20).
- Wessel, P., Smith, W.H.F., Scharroo, R., Luis, J., Wobbe, F., 2013. Generic mapping tools: improved version released. *Eos Trans. AGU* 94 (45), 409.
- Wiemer, S., 2001. A software package to analyze seismicity: ZMAP. *Seismol. Res. Lett.* 72 (3), 373–382.
- Wu, C., Meng, X., Peng, Z., Ben-Zion, Y., 2014. Lack of spatio-temporal localization of foreshocks before the 1999 M_w 7.1 Duzce, Turkey earthquake. *Bull. Seismol. Soc. Am.* 104 (1), 560–566. <http://dx.doi.org/10.1785/0120130140>.
- Yao, D., Walter, J., Meng, X., Peng, Z., Schwartz, S., Protti, M., 2014. Postseismic Slip Inferred from Repeating Earthquakes Following the 2012 M_w 7.6 Nicoya Earthquake in Costa Rica. Abstract G43B-0509. In: 2014 Fall Meeting. 15–19 Dec. AGU, San Francisco, Calif.
- Yao, D., Peng, Z., Meng, X., 2015. Systematical search for remotely triggered earthquakes in Tibetan Plateau following the 2004 M 9.0 Sumatra and 2005 M 8.6 Nias earthquakes. *Geophys. J. Int.* 201 (2), 543–551. <http://dx.doi.org/10.1093/gji/ggv037>.
- Yue, H., et al., 2013. The 5 September 2012 Costa Rica M_w 7.6 earthquake rupture process from joint inversion of high-rate GPS, strong-motion, and teleseismic P wave data and its relationship to adjacent plate boundary interface properties. *J. Geophys. Res.* 118, 5453–5466.
- Zhang, H., Thurber, C.H., 2003. Double-difference tomography: the method and its application to the Hayward fault, California. *Bull. Seismol. Soc. Am.* 93, 1875–1889.